Synthesis of nanocrystalline eskolaite *via* grimaldiite

Marko Robić[1], Mira Ristić[1], Stjepko Krehula[1], Marijana Jurić[1], Svetozar Musić[1,2,*]

Abstract

Grimaldiite (α-CrOOH) was precipitated hydrothermally from the $CrCl_3$ aqueous solution in the presence of hexamethylenetetramine (HMTA). The crystallite size of grimaldiite samples was estimated to be ~2 nm. Eskolaite (α-Cr_2O_3) was produced by the calcination of grimaldiite at 500 and 700°C. FE-SEM images showed amorphous-like aggregates of grimaldiite due to very fine particles (crystallites), whereas eskolaite was in the form of sphere-like nanoparticles. Synthesized grimaldiite and eskolaite were used in the investigation of rhodamine B (RhB) degradation. The significant degradation percentage of RhB obtained by grimaldiite was explained as catalytic effect (in dark) and photocatalytic contribution (with illumination).

Keywords: grimaldiite, eskolaite, HMTA, nanocrystallinity, rhodamine B

Mira Ristić (†): Deceased

✉ Svetozar Musić
music@irb.hr

[1]Division of Materials Chemistry, Rudjer Bošković Institute, Bijenička cesta 54, HR-10000, Croatia
[2]Croatian Academy of Science and Arts, Zrinski trg 11, HR-10000 Zagreb, Croatia

Introduction

Synthetic eskolaite (α-Cr_2O_3) is an important technological material with many applications. It can be used as a green pigment, whereas very small Cr_2O_3 particles can be used as a transparent colorant. Furthermore, there are applications of Cr_2O_3 in heterogeneous catalysis or as a possible sensing material. The Cr_2O_3 phase is important in many mixed metal oxide composites. Specific acido-basic surface properties make it an interesting adsorption material. Due to its high melting temperature (~2435°C) Cr_2O_3 is also an important refractory material. For these reasons it is not surprising that many researchers investigated Cr_2O_3 and CrOOH precursors from different aspects.

In reference literature different chemical and physical methods of Cr_2O_3 synthesis were applied. A simple method based on the hydrothermal treatment of the precipitate obtained by adding alkali to the Cr(III) salt solution was reported (Ratnasamy and Léonard 1972; Vayssieres and Manthiram 2003; Onjia et al. 2003; Kim et al. 2004; Yang et al. 2010). Thermal decomposition of chromium oxyhydroxide was also utilized to prepare Cr_2O_3 particles (Kittaka et al. 1985; Liang et al. 2014; Pardo et al. 2017). Tsuzuki and McCormick (2000) synthesized Cr_2O_3 particles by mechanochemical processing of the $Na_2Cr_2O_7$+S mixture, followed by calcination at 520°C. Bai et al. (2006) used the reductive conversion of K_2CrO_4 with H_2 at 500°C to prepare Cr_2O_3 particles with a mean diameter ~0.3 μm. Cr_2O_3 nanoparticles were prepared hydrothermally by reducing CrO_3 with HCHO or C_2H_5OH (Pei et al. 2009). Eskolaite (α-Cr_2O_3) was also synthesized using activated carbon as a reductant for Cr(VI) and template (Cruz-Espinoza et al. 2012; Ibarra-Galván et al. 2014). Electrospun Cr_2O_3 nanofibres were also synthesized and tested as sensor response towards C_2H_5OH (Hao et al. 2006). Deposition techniques were mainly used in the preparation of thin Cr_2O_3 films (Cheng et al. 1996).

The above short literature review shows very different methods used in the synthesis of Cr_2O_3. These works showed a dependence of Cr_2O_3 properties on the synthesis method.

In the present work we report new results about the hydrothermal synthesis of very fine grimaldiite (α-CrOOH) particles and their transformation to eskolaite (α-Cr_2O_3) by calcination. Hexamethylenetetramine (HMTA) was used as a precipitating agent. The properties of α-Cr_2O_3 are depending on the chemical and physical properties of the

precursor. In the present work the conditions for homogenous precipitation of α-CrOOH are achieved by applying the hydrothermal decomposition of HMTA. Due to the search for new energy materials, as well as those for the pollution decontamination there are specific interests of researchers in the chemistry and physics of metal oxides.

Experimental

Chromium (III)-chloride hexahydrate (99.5% min) by *Alpha Aesar*® and HMTA p.a. by *Kemika* (Zagreb, Croatia) were used in the synthesis. A Commercial Cr_2O_3 325 mesh by *Alfa Aesar*® was also used. The precipitation systems were hydrothermally treated at 160°C using a Teflon®-lined, non-stirred pressure vessel manufactured by *Paar Instruments* (model 4744). The autoclaves were heated in a DX 300 gravity oven (Yamato, temperature uniformity ±1.9°C at 100°C and ±3°C at 200°C). The autoclaving times were corrected for the time needed that the autoclave reaches predetermined temperature. Experimental conditions for the synthesis of very fine grimaldiite particles are given in Table 1. Thus obtained precipitates were kept for 3 days at RT, then washed with double-distilled water and dried (24h) in the laboratory dryer at ~100°C. Dried precipitates were calcined in air at 500 and 700°C (10°C/min) in crucibles.

XRD patterns were recorded with a *Panalytical Aeris* powder diffractometer using Cu$K\alpha_{1,2}$ radiation. The crystallite sizes were determined using the well-known Scherrer formula (Match! program).

FT-IR spectra were recorded using a Frontier spectrometer manufactured by *Perkin Elmer*. The spectra were recorded in the ATR mode.

Optical spectra were recorded using a *Shimadzu* 3600 spectrometer.

DTA/TGA curves were recorded with a Shimadzu DTG-60H in synthetic air.

FE-SEM scanning electron microscope (model JSM-7000F) manufactured by *JEOL* Ltd was used.

Photocatalytic measurements were conducted with a MAX-303-Compact Xenon light source with 300 W lamps manufactured by *Asahi Spectra*. The apparatus was supplied with adequate filters (420 nm). The procedure for photocatalytic measurements was described elsewhere (Robić et al. 2020). A standard photocatalytic test for the

degradation of rhodamine B was carried out using 30% H_2O_2 by *Kemika* (Zagreb, Croatia) and rhodamine B (RhB) by *Merck*.

Degradation of RhB (coloured organic material) was used, because in such a way it is easy to compare catalytic or photocatalytic activities of various materials (for example, hematite, titania, doped metal oxides etc.).

Results and discussion

In the present work HMTA (hexamethylenetetramine) was used, because this compound undergoes homogenous hydrolysis in the water medium in line with chemical reactions:

$$C_6H_{12}N_4 + 6H_2O \rightarrow 6HCHO + 4NH_3 \quad (1)$$

and

$$NH_3 + H_2O \rightarrow NH_4^+ + OH^-, \quad (2)$$

thus gradually increasing the pH of the solution. At room temperature the kinetics of these reactions is slow; however, with temperature rise the hydrolysis of HMTA is significantly increased. The application of these reactions to the forced hydrolysis of metal cations may create uniform conditions for the precipitation of different metal cations. For example, typical studies of the precipitation of oxyhydroxides and oxides of Fe^{3+} ions were conducted in the presence of HMTA (Šarić et al. 1998; Musić et al. 1997). The solid phases obtained by the hydrothermal precipitation of Cr^{3+} ions in the presence of HMTA and upon calcination were analyzed as follows.

Figure 1 shows the XRD patterns of samples A and B. Very broad XRD lines are well visible, thus indicating the presence of very fine crystallites. The reference XRD patterns of grimaldiite, chromium hydroxide hydrate, guyanaite and bracewelite are also shown in the same Figure. Taking into consideration these reference XRD patterns it can be concluded that samples A and B correspond to the grimaldiite (α-CrOOH) phase.

Figure 2 shows the XRD patterns of samples A and B upon heating at 500 and 700°C, respectively. In the same Figure the XRD patterns of commercial Cr_2O_3 as well as reference eskolaite are also shown. Crystallite sizes D of samples A and B and their calcination products are calculated using the Scherrer formula:

$$D = \frac{K \cdot \lambda}{\beta \cdot \cos\theta} \quad (3)$$

where D = crystallite size, λ = wavelength of CuKα line, β = full-width at half maximum of the diffraction peak, θ = position of the peak and constant K =0.94. The estimated D values are given in Table 2. It is visible that the crystallite sizes D of samples A and B are approximately 2 nm, whereas the crystallite sizes of calcination products are greater, but also in the nanosize range. The increase in the Cr_2O_3 crystallite size from 500 to 700°C is also visible.

DTA/TGA curves of samples A and B recorded in synthetic air are shown in Figure 3. The endo peak at ~100°C can be assigned to the release of moisture present in samples A and B, whereas exo peaks at 278 and 355°C can be assigned to a partial loss of –OH groups. The α-CrOOH to α-Cr_2O_3 phase transformation is characterized with a strong exo peak at 414 cm^{-1}. Musić et al. (1999) noticed the transformation of amorphous chromium hydroxide to Cr_2O_3 between 410 and 420°C, in dependence on the preparation.

FT-IR spectra of samples A, B and reference HMTA powder are shown in Figure 4. The spectra of obtained samples A and B show the same feature. No peaks of residual HMTA in these samples are visible. The IR band at 452 cm^{-1} can be assigned to the vibration of a chromium-oxygen bond. In the same spectrum two IR bands centered at 899 and 796 cm^{-1} were also noticed. Ratnasamy and Léonard (1972) recorded the IR spectra of calcination products of amorphous chromium hydroxide gel which were heated up to 900°C. These authors also noticed the formation of two IR bands in the region approximately 800 to 900 cm^{-1} for samples heated between 100 and 240°C. Abecassis-Wolfovich et al. (2003) reported the FT-IR spectra of α-CrOOH thermally treated under different conditions. Two broad IR bands centered at 940 and 772 cm^{-1} and a very strong IR band at 543 cm^{-1} were noticed upon the supercritical extraction with CO_2 and the additional evacuation at 320°C. The IR band at 1623 cm^{-1} can be related with bending mode of H_2O molecules (moisture). The IR bands in the range 1462 to 1062 cm^{-1} (noticed in Figure 4) can be assigned to specifically adsorbed carbonate/bicarbonate on grimaldiite as picked up during the washing procedure and drying the precipitates at ~100°C. This is possible because the experiments were not performed in a CO_2-free atmosphere and using the CO_2-free water. Moreover, CO_2 can be released due to the decomposition of formaldehyde at temperatures higher than 150°C. FT-IR spectra of samples A and B did not show the presence of formaldehyde. More about the reactions of

carbonate/bicarbonate ions with metal oxide surfaces can be found in corresponding literature (Fukuda and Tanabe 1973, Wijnja and Schulthess 1999, Garand et al. 2010, Su and Suarez 1997).

Figure 5 shows the FT-IR spectra of calcination products obtained at 500 and 700°C, respectively. The reference spectrum of commercial Cr_2O_3 is also shown. All calcined products show IR bands typical of Cr_2O_3. Renneke and Lynch (1965) reported the IR modes of Cr_2O_3 vibrating parallel to the *c*-axis at 538 and 613 cm^{-1}, whereas the modes vibrating perpendicular to the c-axis were located at 417, 444, 532 and 613 cm^{-1}. Serna et al. (1982) investigated the influence of the Cr_2O_3 shape on the corresponding IR spectrum. For the dominant lath-like particles the bands at 617, 556, 443 and 305 cm^{-1} were assigned to E_u modes, whereas the bands at 415 and ~720 cm^{-1} were assigned to A_{2u} modes. Small contributions of cylinder- or sphere- type particles were related to the broad shoulder at 650 to 700 cm^{-1}.

Figure 6 shows the FE SEM images of samples A and B and those produced by calcination at 500 and 700°C. Samples A and B are in the form of big aggregates without visible specific morphology. This is due to very fine crystallite particles as shown in Table 2. Samples produced by calcination at 500 and 700°C consist of fine sphere-like nanoparticles.

The photocatalytic activities of prepared samples were investigated and the typical results are shown in Figures 7, 8 and 9 as illustrated with samples B, B-500 and B-700. Figure 7 shows that a significant degradation of RhB occurred when the system containing grimaldiite (sample B) was kept in dark (no illumination). When the same system was illuminated the degradation of RhB further increased (83.5 % after 3h). Evidently, grimaldiite nanoparticles in dark acted as catalyst for degradation of RhB, whereas under the illumination there is additionally the photocatalytic activity. The high percentage of RhB degradation can be assigned not just to the chemical nature of grimaldiite, but also to the presence of very fine particles (crystallites). It is also possible that the surface oxidation of Cr(III) with H_2O_2 has some influence on the degradation process of RhB. Figure 8 shows changes in the visible part of the spectrum during the degradation of RhB in the dark as well as under illumination. Figure 9 shows the

degradation of RhB with samples B-500 and B-700. These samples, consisting of α-Cr_2O_3, showed much less degradation of RhB than it was the case with grimaldiite.

Conclusion

Hydrothermal precipitation at 160°C was utilized to synthesize grimaldiite (α-CrOOH) from the $CrCl_3$ solution in the presence of hexamethylenetetramine (HMTA). Accelerated HMTA hydrolysis was used to generate OH^- ions for a homogenous precipitation. The Scherrer formula was applied to estimate the crystallite size (~2nm) of grimaldiite samples. Calcination of grimaldiite produced eskolaite (α-Cr_2O_3). FE SEM images of grimaldiite showed the presence of an amorphous-like structure due to the presence of very fine particles (crystallite). On the other hand, FE SEM images of eskolaite showed the presence of sphere-like nanoparticles. Surprisingly, grimaldiite nanoparticles (very fine crystallites) showed a high percentage of RhB degradation in dark by acting as catalyst. Under the illumination of test solution RhB degradation was additionally increased. Using also the standard photocatalytic test eskolaite nanoparticles showed much less degradation of RhB.

Figure legends

Figure 1 XRD patterns of samples A, B and reference patterns of grimaldiite, chromium hydroxide hydrate, guyanaite and bracewellite

Figure 2 XRD patterns of samples A-500, B-500, A-700 and B-700 obtained by calcination of grimaldiite at 500 and 700°C, respectively. XRD patterns of a commercial Cr_2O_3 325 mesh and reference eskolaite are also shown

Figure 3 DTA/TGA curves of samples A and B recorded in synthetic air

Figure 4 FT-IR spectra of samples A and B and reference HMTA powder

Figure 5 FT-IR spectra of eskolaite (α-Cr_2O_3) obtained by calcination of grimaldiite (α-CrOOH) at 500 and 700°C, respectively

Figure 6 FE SEM images of samples, A, B, A-500, B-500, A-700 and B-700

Figure 7 Degradation of rhodamine B by grimaldiite (sample B) without illumination (in darkness) and with illumination

Figure 8 Changes in the visible part of the optical spectrum during the degradation of rhodamine B by grimaldiite: (a) without illumination (in dark), (b) with illumination

Figure 9 Degradation of rhodamine B by eskolaite samples B-500 and B-700. A significant decrease in the activity of eskolaite samples relative to grimaldiite (sample B) is visible

References

Abecassis-Wolfovich M, Rotter H, Landau MV, Korin E, Erenburg AI, Mogilyansky D, Gartstein E (2003) Texture and nanostructure of chromia aerogels prepared by urea-assisted homogeneous precipitation and low-temperature supercritical drying. J Non Cryst Solids 318:95–111. https://doi.org/10.1016/S0022-3093(02)01881-1

Bai YL, Xu H Bin, Zhang Y, Li ZH (2006) Reductive conversion of hexavalent chromium in the preparation of ultra-fine chromia powder. J Phys Chem Solids 67:2589–2595. https://doi.org/10.1016/j.jpcs.2006.07.018

Cheng CS, Gomi H, Sakata H (1996) Electrical and optical properties of Cr_2O_3 films prepared by chemical vapour deposition. Phys Status Solidi Appl Res 155:417–425. https://doi.org/10.1002/pssa.2211550215

Cruz-Espinoza A, Ibarra-Galván V, López-Valdivieso A, González-González J (2012) Synthesis of microporous eskolaite from Cr(VI) using activated carbon as a reductant and template. J Colloid Interface Sci 374:321–324. https://doi.org/10.1016/j.jcis.2012.01.059

Fukuda Y, Tanabe K (1973) Infrared Study of Carbon Dioxide Adsorbed on Magnesium and Calcium Oxides. Bull. Chem. Soc. Jpn. 46:1616–1619, https://doi.org/10.1246/bcsj.46.1616

Garand E, Wende T, Goebbert DJ, Bergmann R, Meijer G, Neumark DM, Asmis KR (2010) Infrared Spectroscopy of Hydrated Bicarbonate Anion Clusters: $HCO3^-(H_2O)_{1-10}$. J Am Chem Soc 132:849–856. https://doi.org/10.1021/ja9093132

Hao R, Yuan J, Peng Q (2006) Fabrication and sensing behavior of Cr_2O_3 nanofibers via in situ gelation and electrospinning. Chem Lett 35:1248–1249. https://doi.org/10.1246/cl.2006.1248

Ibarra-Galván V, López-Valdivieso A, Villavelazquez-Mendoza CI, Santoyo-Salazar J, Song S (2014) Synthesis of eskolaite (α-Cr_2O_3) nanostructures by thermal processing of Cr_2O_3-loaded activated carbon. Part Sci Technol 32:451–455. https://doi.org/10.1080/02726351.2013.878774

Kim DW, Shin S Il, Lee JD, Oh SG (2004) Preparation of chromia nanoparticles by precipitation-gelation reaction. Mater Lett 58:1894–1898. https://doi.org/10.1016/j.matlet.2003.11.023

Kittaka S, Morooka T, Kitayama K, Morimoto T (1985) Thermal decomposition of chromium oxide hydroxide. J Solid State Chem 58:187–193. https://doi.org/10.1016/0022-4596(85)90234-8

Liang ST, Zhang HL, Luo MT, Luo KJ, Li P, Xu HB, Zhang Y (2014) Colour performance investigation of a Cr_2O_3 green pigment prepared via the thermal decomposition of CrOOH. Ceram Int 40:4367–4373. https://doi.org/10.1016/j.ceramint.2013.08.107

Musić S, Maljković M, Popović S, Trojko R (1999) Formation of chromia from amorphous chromium hydroxide. Croat Chem Acta 72:789–802

Musić S, Šarić A, Popović S (1997) Effects of urotropin on the formation of β-FeOOH. J Mol Struct 410–411:153–156. https://doi.org/10.1016/S0022-2860(96)09576-2

Onjia AE, Milonjić SK, Čokeša D, Čomor M, Miljević N (2003) Characterization of colloidal chromia particles obtained by forced hydrolysis. Mater Res Bull 38:1329–1339. https://doi.org/10.1016/S0025-5408(03)00137-5

Pardo P, Calatayud JM, Alarcón J (2017) Chromium oxide nanoparticles with controlled size prepared from hydrothermal chromium oxyhydroxide precursors. Ceram Int 43:2756–2764. https://doi.org/10.1016/j.ceramint.2016.11.104

Pei Z, Xu H, Zhang Y (2009) Preparation of Cr_2O_3 nanoparticles via C_2H_5OH hydrothermal reduction. J Alloys Compd 468:2007–2010. https://doi.org/10.1016/j.jallcom.2007.12.086

Pei Z, Zhang Y (2008) A novel method to prepare Cr_2O_3 nanoparticles. Mater Lett 62:504–506. https://doi.org/10.1016/j.matlet.2007.05.073

Ratnasamy P, Léonard AJ (1972) Structural evolution of chromia. J Phys Chem 76:1838–1843. https://doi.org/10.1021/j100657a009

Renneke DR, Lynch DW (1965) Infrared lattice vibrations and dielectric dispersion in single-crystal Cr_2O_3. Phys Rev 138:. https://doi.org/10.1103/PhysRev.138.A530

Robić M, Ristić M, Marciuš M, Krehula S, Musić S (2020) Synthesis and properties of nanostructured Cr - doped hematite fibres. Chem Pap. https://doi.org/10.1007/s11696-020-01247-6

Šarić A, Nomura K, Popović S, Ljubešić N, Musić S (1998) Effects of urotropin on the chemical and microstructural properties of Fe-oxide powders prepared by the hydrolysis of aqueous $FeCl_3$ solutions. Mater Chem Phys 52:214–220.

https://doi.org/10.1016/S0254-0584(97)02032-4

Serna CJ, Rendon JL, Iglesias JE (1982) Infrared surface modes in corundum-type microcrystalline oxides. Spectrochim Acta Part A Mol Spectrosc 38:797–802. https://doi.org/10.1016/0584-8539(82)80070-6

Su C, Suarez DL (1997) In situ infrared speciation of adsorbed carbonate on aluminum and iron oxides. Clays Clay Miner 45:814–825. https://doi.org/10.1346/CCMN.1997.0450605

Tsuzuki T, McCormick PG (2000) Synthesis of Cr_2O_3 nanoparticles by mechanochemical processing. Acta Mater 48:2795–2801. https://doi.org/10.1016/S1359-6454(00)00100-2

Vayssieres L, Manthiram A (2003) 2-D mesoparticulate arrays of α-Cr_2O_3. J Phys Chem B 107:2623–2625. https://doi.org/10.1021/jp026933u

Wijnja H, Schulthess CP (1999) ATR-FTIR and DRIFT spectroscopy of carbonate species at the aged γ-Al_2O_3/water interface. Spectrochim Acta - Part A Mol Biomol Spectrosc 55:861–872. https://doi.org/10.1016/S1386-1425(98)00236-4

Yang J, Baker AG, Liu H, Martens WN, Frost RL (2010) Size-controllable synthesis of chromium oxyhydroxide nanomaterials using a soft chemical hydrothermal route. J Mater Sci 45:6574–6585. https://doi.org/10.1007/s10853-010-4746-3

Table 1 Experimental conditions for the synthesis of samples A and B

Sample	$CrCl_3$ / M	HMTA / M	T / °C	t / h	pH_{start}	pH_{final}
A	0.1	0.25	160	24	5.11	9.23
B	0.2	0.25	160	24	4.83	7.82

HMTA= Hexamethylenetetramine (Urotropin)

Table 2 Estimated crystallite sizes of samples A and B and their calcination products

Sample	R_p / %	Crystallite size* / nm
A	10.7	2.2
A-500	2.3	18.2
A-700	1.8	24.0
B	9.7	1.8
B-500	2.6	18.7
B-700	2.5	33.3

*LaB_6 standard was used.

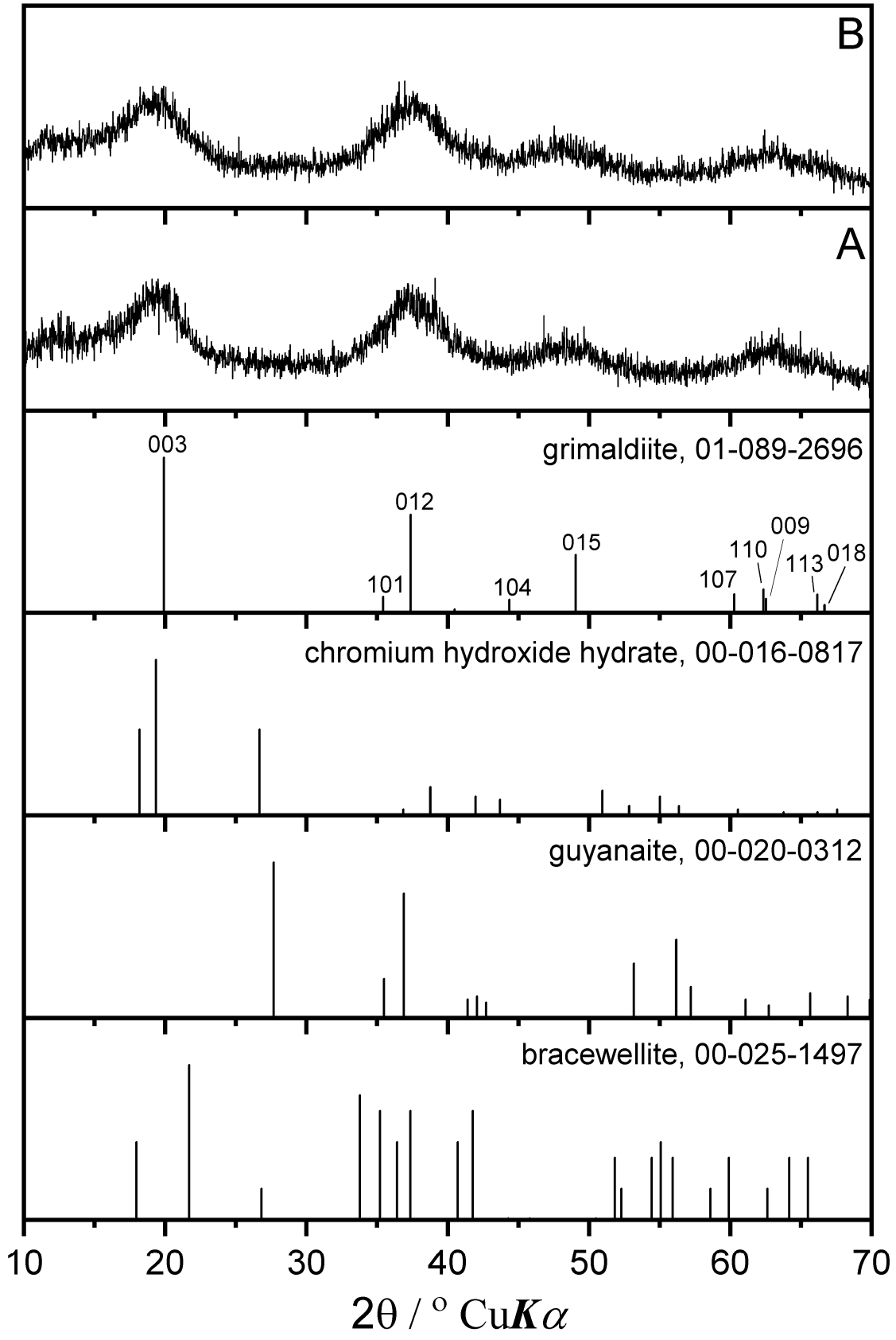
B
A
grimaldiite, 01-089-2696
003
012
101
104
015
107
110
009
113
018
chromium hydroxide hydrate, 00-016-0817
guyanaite, 00-020-0312
bracewellite, 00-025-1497
10
20
30
40
50
60
70
2θ / ° CuKα

Figure 1

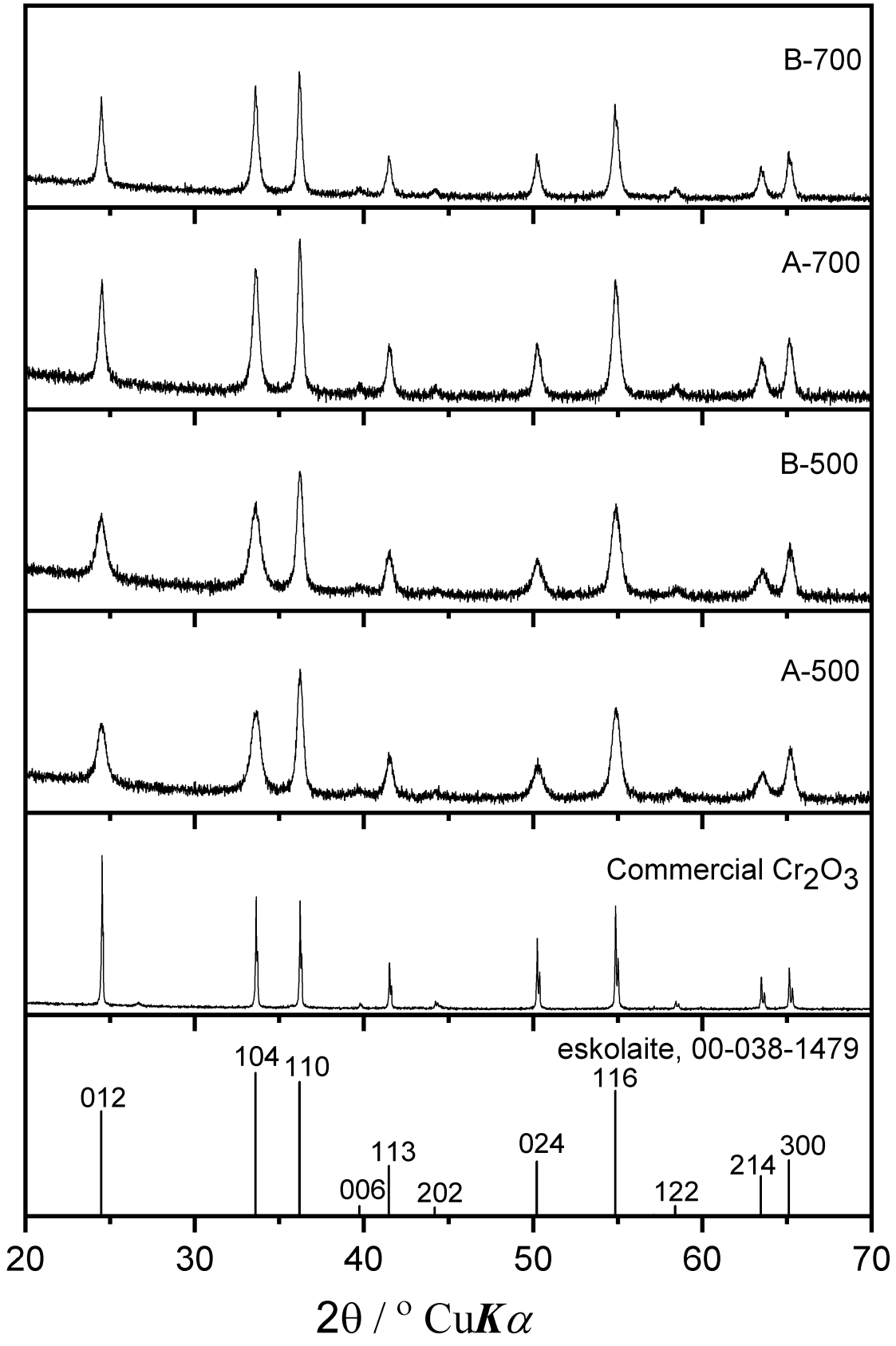
B-700
A-700
B-500
A-500
Commercial Cr_2O_3
eskolaite, 00-038-1479
012
104
110
006
113
202
024
116
122
214
300
20
30
40
50
60
70
2θ / ° Cu$K\alpha$

Figure 2

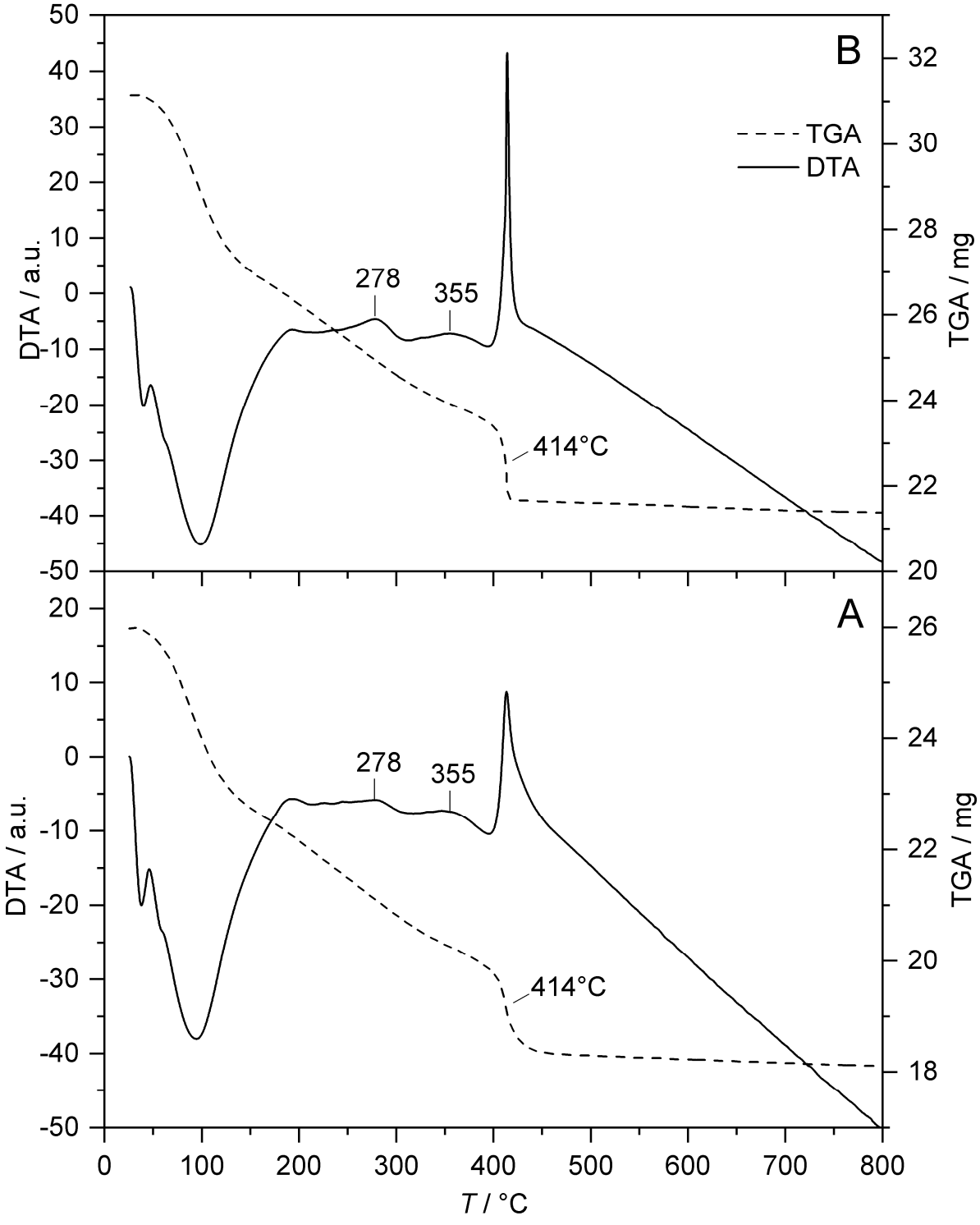

Figure 3

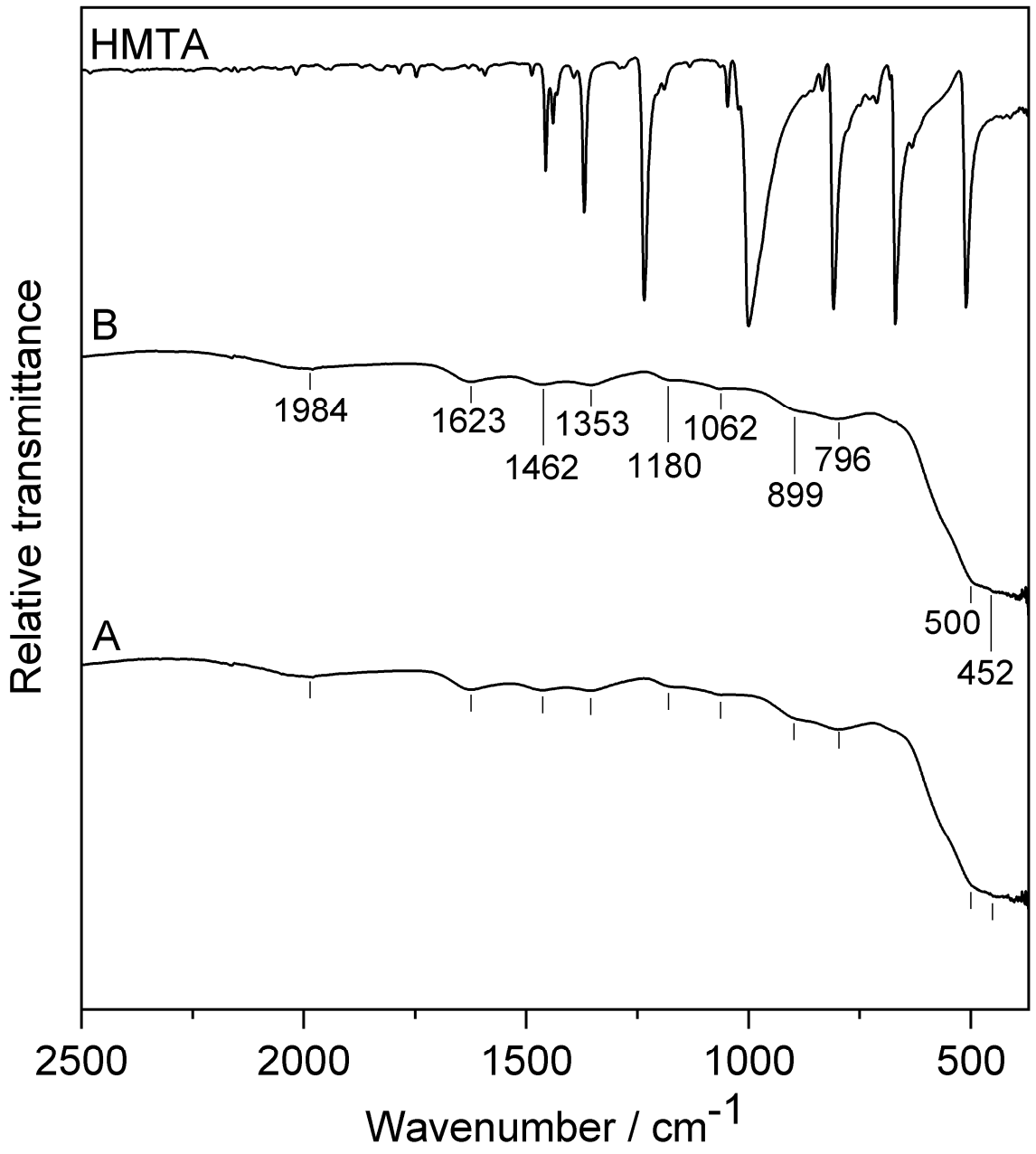
HMTA
B
A
1984
1623
1462
1353
1180
1062
899
796
500
452
Relative transmittance
2500
2000
1500
1000
500
Wavenumber / cm-1

Figure 4

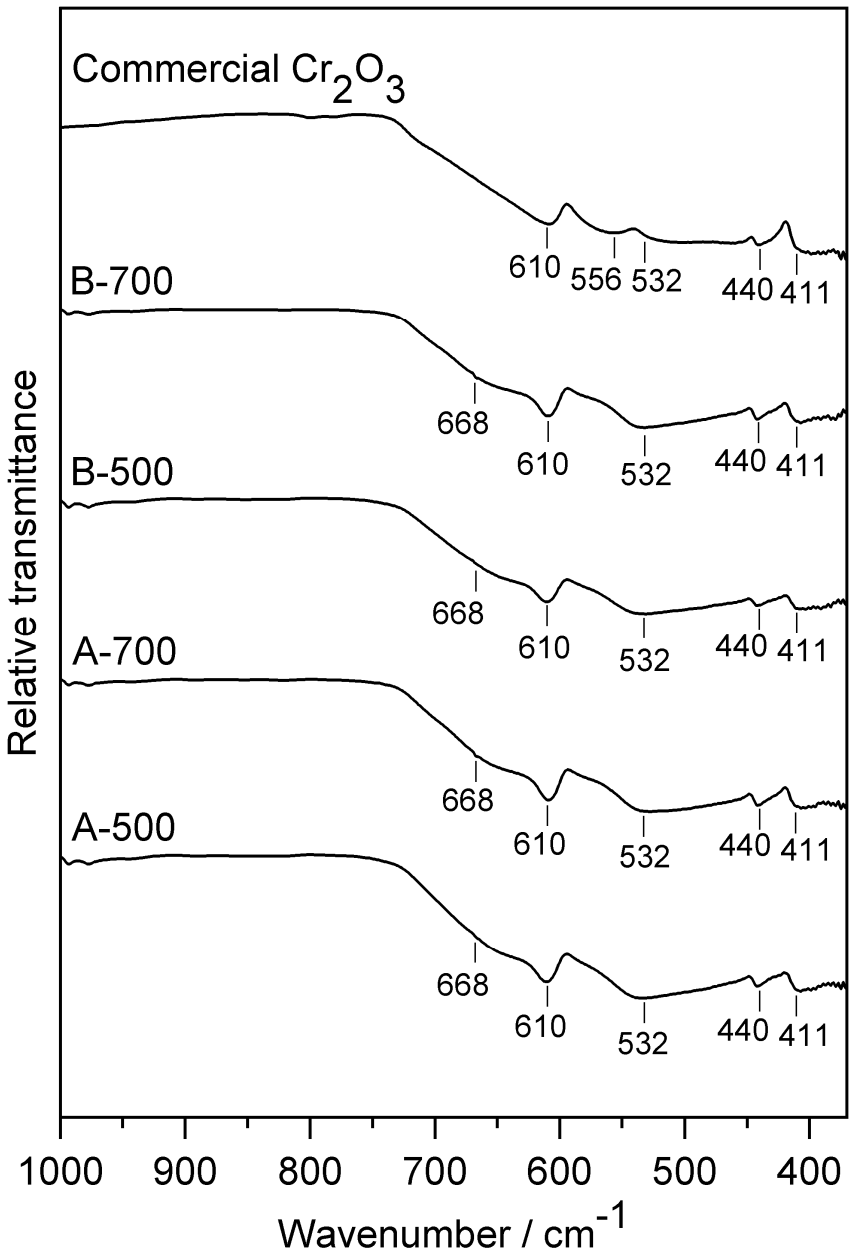
Commercial Cr_2O_3
610
556
532
440
411
B-700
668
610
532
440
411
B-500
668
610
532
440
411
A-700
668
610
532
440
411
A-500
668
610
532
440
411
Relative transmittance
1000
900
800
700
600
500
400
Wavenumber / cm^{-1}

Figure 5

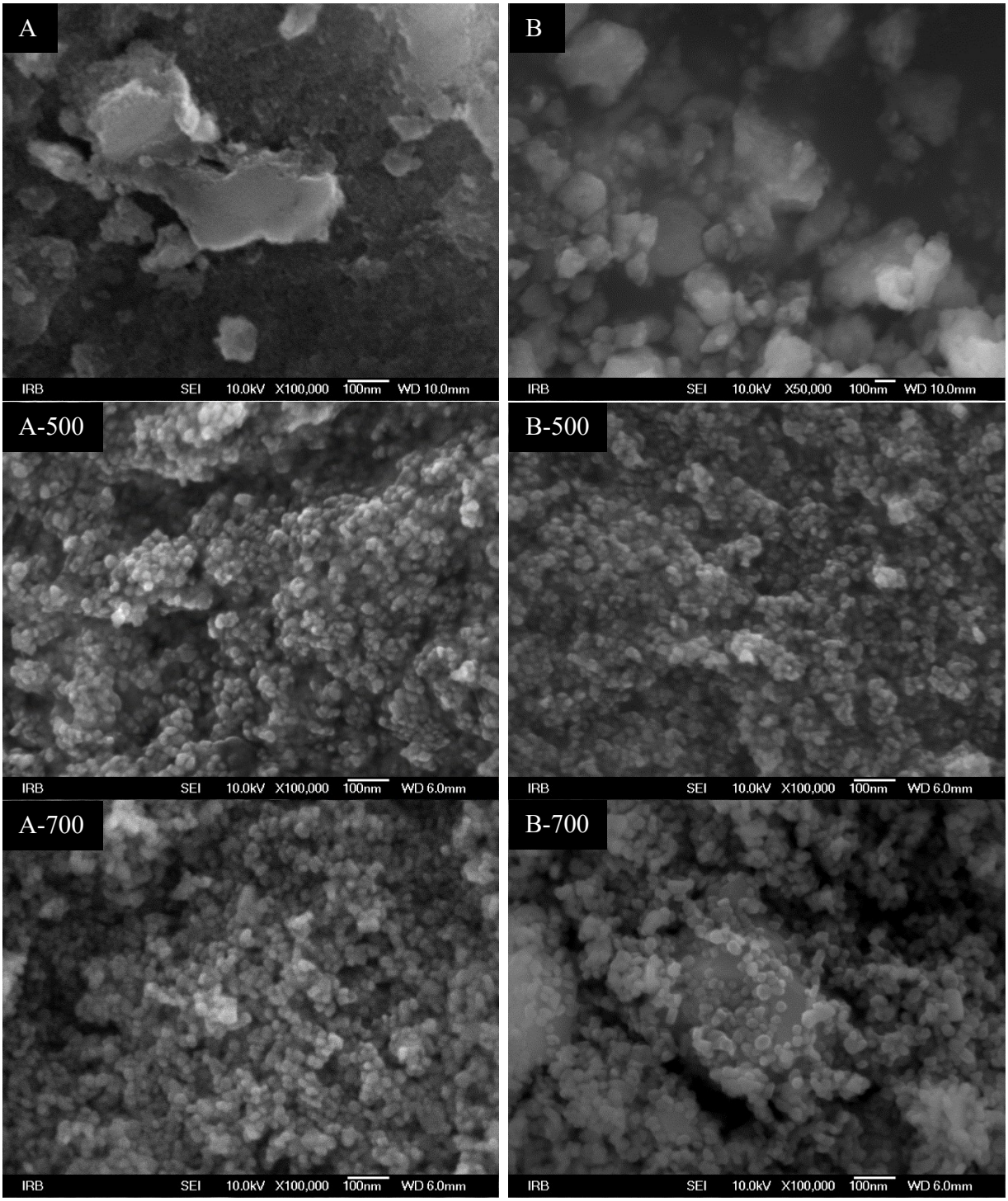
A
IRB SEI 10.0kV X100,000 100nm WD 10.0mm
B
IRB SEI 10.0kV X50,000 100nm WD 10.0mm
A-500
IRB SEI 10.0kV X100,000 100nm WD 6.0mm
B-500
IRB SEI 10.0kV X100,000 100nm WD 6.0mm
A-700
IRB SEI 10.0kV X100,000 100nm WD 6.0mm
B-700
IRB SEI 10.0kV X100,000 100nm WD 6.0mm

Figure 6

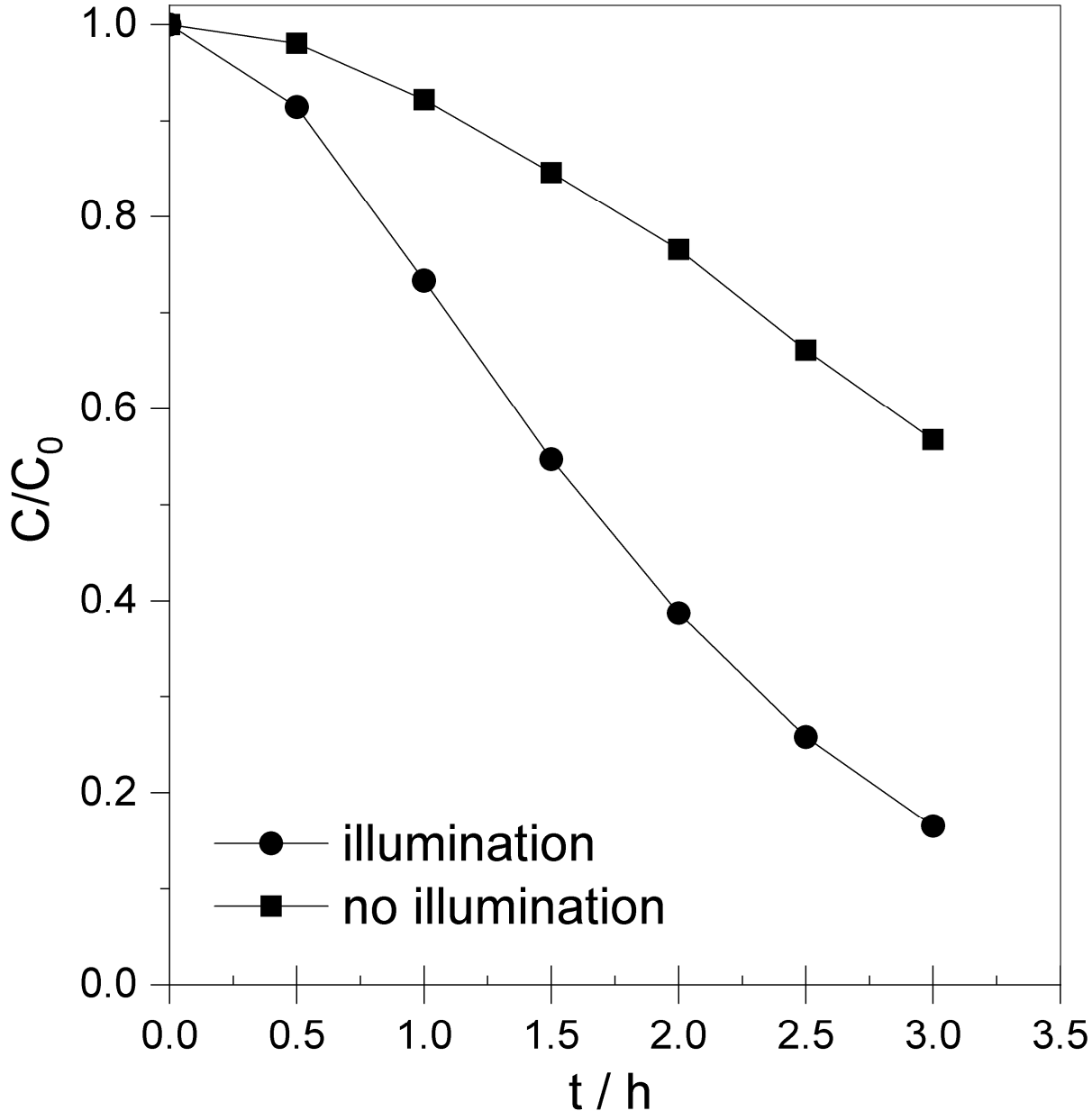
1.0
0.8
0.6
0.4
0.2
0.0
C/C0
0.0
0.5
1.0
1.5
2.0
2.5
3.0
3.5
t / h
illumination
no illumination

Figure 7

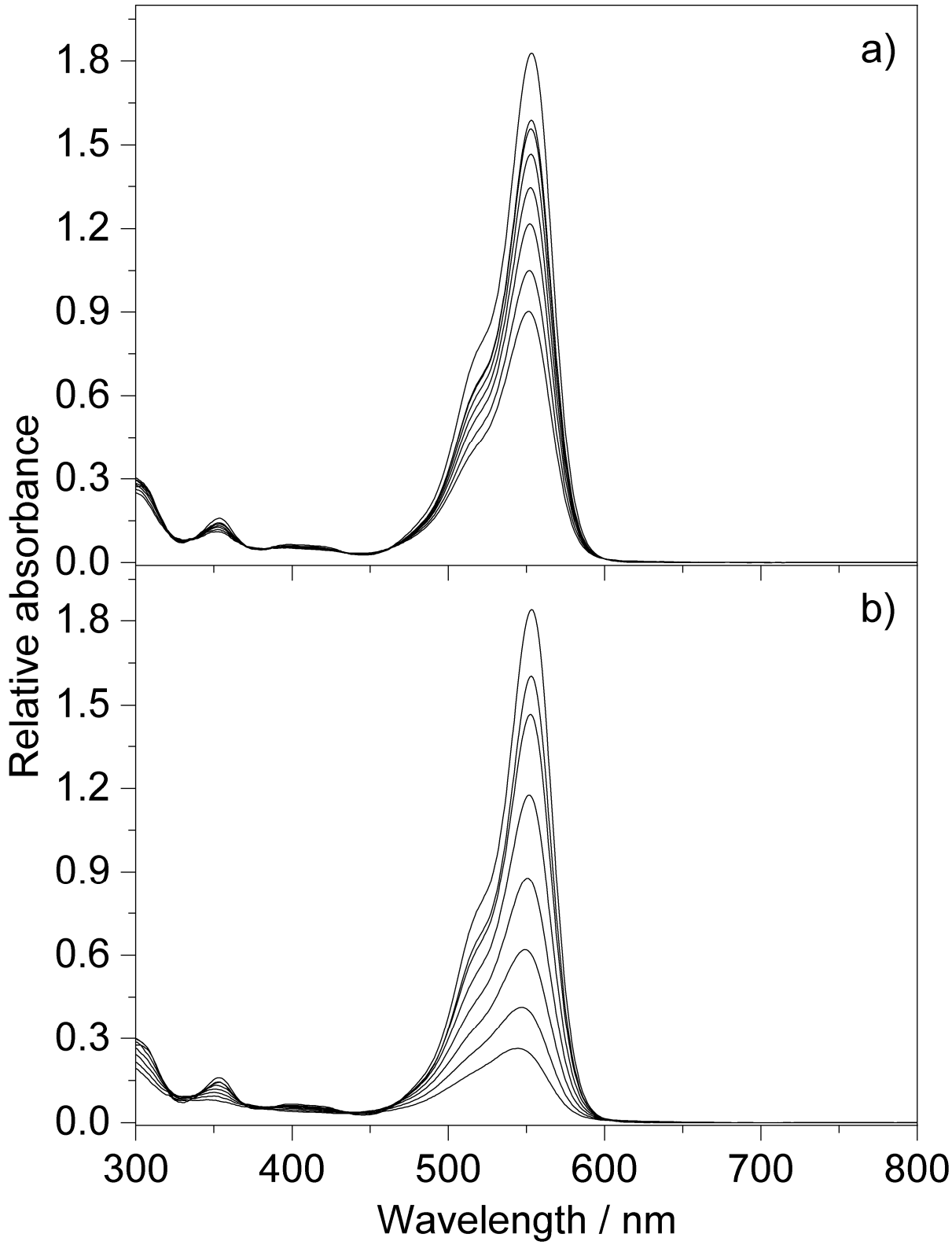
a)
b)
Relative absorbance
0.0
0.3
0.6
0.9
1.2
1.5
1.8
300
400
500
600
700
800
Wavelength / nm

Figure 8

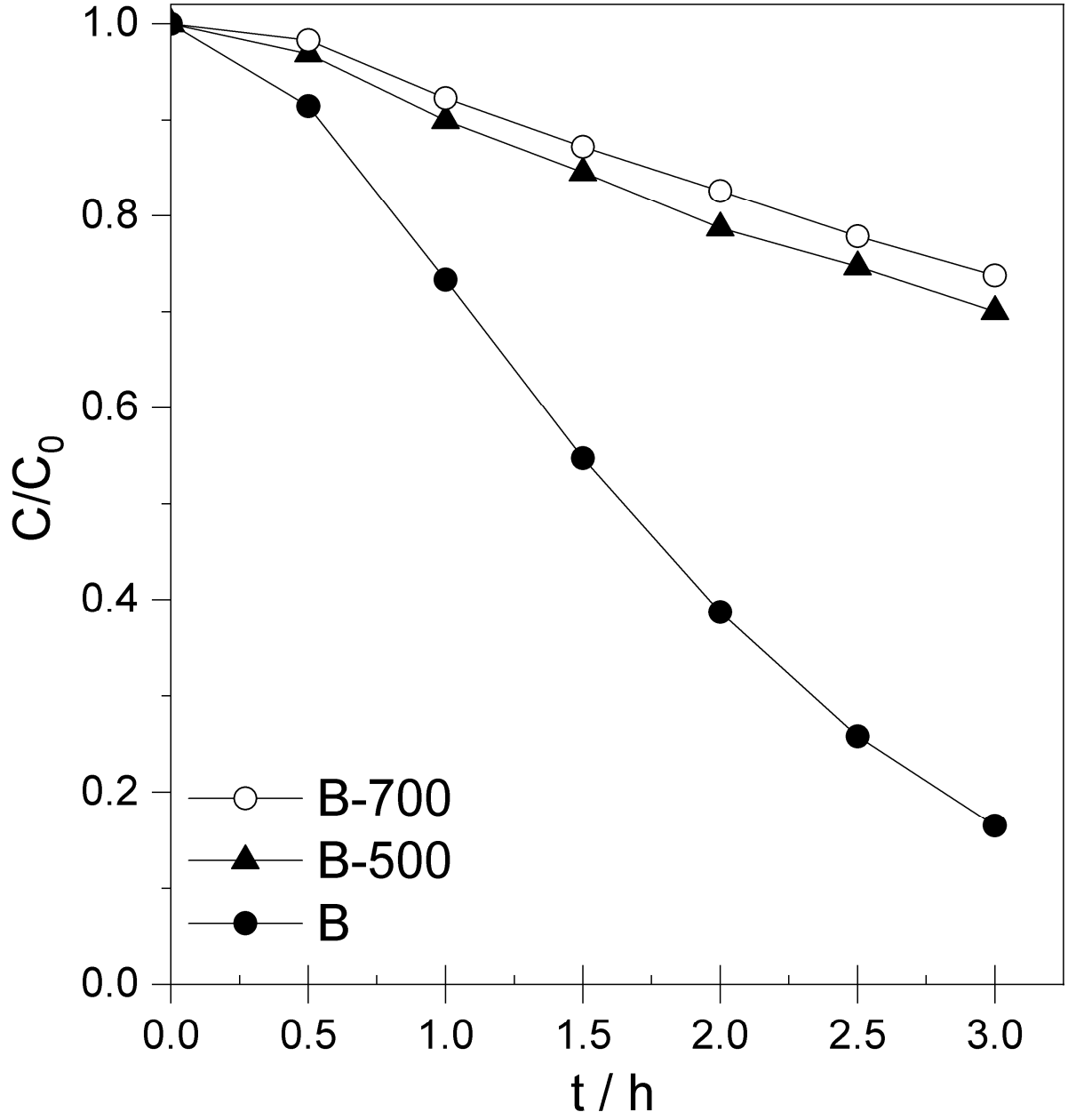

Figure 9